Synthesis and X-ray Characterization of the Phosphido−Carbonyl Cluster Anions $[Co_9(\mu_8\text{-}P)(CO)_{21}]^{2-}$ and $[Co_{10}(\mu_8\text{-}P)(CO)_{22}]^{3-}$

Gianfranco Ciani,[†] Angelo Sironi,*[,†] Secondo Martinengo,[‡,§] Luigi Garlaschelli,*[,‡] Roberto Della Pergola,[#] Piero Zanello,[¶] Franco Laschi,[¶] and Norberto Masciocchi[£]

Dipartimento di Chimica Strutturale e Stereochimica Inorganica and Centro CNR, Via G. Venezian 21, 20133 Milano, Italy, Dipartimento di Chimica Inorganica, Metallorganica e Analitica and Centro CNR, Via G. Venezian 21, 20133 Milano, Italy, Dipartimento di Scienze dell' Ambiente e del Territorio, piazza della Scienza 1, 20126 Milano, Italy, Dipartimento di Chimica dell'Università di Siena, via Aldo Moro, 53100 Siena, Italy, and Dipartimento di Scienze Chimiche, Fisiche e Matematiche, via Valleggio 11, 22100 Como, Italy

Received July 3, 2000

The $[Co_9P(CO)_{21}]^{2-}$ anion has been isolated from the products of the reaction between $Na[Co(CO)_4]$ and PCl_5 in tetrahydrofuran at reflux. The structure of the cluster anion $[Co_9P(CO)_{21}]^{2-}$ in its tetraphenylphosphonium salt has been elucidated by X-ray analysis. The crystals are monoclinic, space group $P2_1/n$, $a = 12.528(3)$, $b = 14.711(5)$, $c = 19.312(6)$ Å, $\beta = 93.68(2)°$, $Z = 2$. Final R = 0.065 for 2300 unique reflections having $I > 3\sigma(I)$. The anion, which is disordered about an inversion center, consists of a monocapped square antiprismatic cluster containing an interstitial phosphide and surrounded by 13 terminal and 8 edge-bridging carbonyl ligands. Average values are: Co−Co 2.685 Å, and Co−P 2.256 Å. The $[Co_{10}P(CO)_{22}]^{3-}$ anion has been obtained by condensation of the $[Co_9P(CO)_{21}]^{2-}$ anion with $[Co(CO)_4]^-$ in tetrahydrofuran at reflux. While the $[Co_9P(CO)_{21}]^{2-}$ anion is stable under CO, the $[Co_{10}P(CO)_{22}]^{3-}$ anion is decomposed to $[Co_9P(CO)_{21}]^{2-}$ and $[Co(CO)_4]^-$. The benzyltrimethylammonium salt of the $[Co_{10}P(CO)_{22}]^{3-}$ anion has been studied by X-ray analysis. It gives triclinic crystals, space group $P\bar{1}$, $a = 11.452(3)$, $b = 23.510(6)$, $c = 25.606(4)$ Å, $\alpha = 112.46(1)$, $\beta = 95.79(1)$, $\gamma = 73.548(2)°$, $Z = 4$. Final R = 0.041 for 8600 unique reflections having $I > 3\sigma(I)$. There are two independent trianions in the asymmetric unit, both showing similar geometries, consisting of bicapped square antiprismatic clusters with a central P atom, each bearing 10 terminal and 12 edge-bridging carbonyl ligands, 8 of which, bound to the capping metals, are markedly asymmetric. Average values are: Co−Co 2.678 Å, and Co−P 2.262 Å. Electrochemistry shows that $[Co_9P(CO)_{21}]^{2-}$ and $[Co_{10}P(CO)_{22}]^{3-}$ in acetonitrile solution undergo either a one-electron oxidation or a two-electron reduction. This latter process appears as a single step in the case of the dianion and as two separated one-electron steps in the case of the trianion. All the processes are accompanied by slow chemical complications, thus testifying that no stable redox congeners exist for these phosphide clusters.

Introduction

Within the cobalt subgroup metals, cobalt resembles much more rhodium, in its high tendency to give carbonyl cluster species with interstitial main group elements, than iridium, for which so far no such compounds have been isolated.

The rhodium cluster compounds containing fully encapsulated pnictides include, besides a number of nitrides,[1] the $[Rh_9P(CO)_{21}]^{2-}$,[2] $[Rh_{10}P(CO)_{22}]^{3-}$,[3] $[Rh_{10}As(CO)_{22}]^{3-}$,[4] and $[Rh_{12}Sb(CO)_{27}]^{3-}$ [5] anions. In contrast, for cobalt, only a few nitrides have been characterized; $[Co_6N(CO)_{15}]^-$,[6] $[Co_6N(CO)_{13}]^-$,[7] $[Co_7N(CO)_{15}]^{2-}$,[8] $[Co_{10}N_2(CO)_{19}]$,[4−9] and $[Co_{14}N_3(CO)_{26}]^{3-}$.[10] No interstitial phosphide is known, the only reported species related to this family is the $[Co_6P(CO)_{16}]^-$ anion,[11] which contains an open hexametal array surrounding a semiexposed P atom. Therefore, continuing our investigations on this class of compounds, we have attempted the synthesis of new cobalt phosphide species, which possibly contain interstitial P atoms. We report here the isolation and X-ray characterization of the novel anions $[Co_9P(CO)_{21}]^{2-}$ (**1**) and $[Co_{10}P(CO)_{22}]^{3-}$ (**2**), exhibiting capped square antiprismatic metal cluster geometries, previously found in the corresponding rhodium species and in

* To whom correspondence should be addressed. L.G. e-mail: luigi.garlaschelli@uuimi.it.
† Dipartimento di Chimica Strutturale e Stereochimica Inorganica and Centro CNR. A.S. e-mail: angelo@csmtbo.mi.cnr.it.
‡ Dipartimento di Chimica Inorganica, Metallorganica e Analitica and Centro CNR.
# Dipartimento di Scienze dell' Ambiente e del Territorio.
¶ Dipartimento di Chimica dell'Università di Siena.
£ Dipartimento di Scienze Chimiche, Fisiche e Matematiche.
§ Deceased in August 1999.

(1) Fumagalli, A.; Della Pergola, R. In *Metal Clusters in Chemistry;* Braunstein, P., Oro, L. A., Raithby, P. R. Eds.; Wiley-VCH: Berlin, 1999; p 323.
(2) Vidal, J. L.; Walker, W. E.; Preuett, R. L.; Schoening, R. C. *Inorg. Chem.* **1979**, *18*, 129.
(3) Vidal, J. L.; Walker, W. E.; Schoening, R. C. *Inorg. Chem.* **1981**, *20*, 238.
(4) Vidal, J. L. *Inorg. Chem.* **1981**, *20*, 243.
(5) Vidal, J. L.; Troup, J. H. *J. Organomet. Chem.* **1982**, *213*, 351.
(6) Martinengo, S.; Ciani, G.; Sironi, A.; Heaton, B. T.; Mason, J. *J. Am. Chem. Soc*, **1979**, *101*, 7095.
(7) Ciani, G.; Martinengo, S. *J. Organomet. Chem.* **1986**, *306*, C49.
(8) Ciani, G.; Masciocchi, N.; Sironi, A.; Fumagalli, A.; Martinengo, S. *Inorg. Chem.* **1992**, *31*, 331
(9) Fumagalli, A.; Martinengo, S.; Tasselli, M.; Ciani, G.; Macchi, P.; Sironi, A. *Inorg. Chem.* **1998**, *377*, 2826.
(10) Martinengo, S.; Ciani, G.; Sironi, A. *J. Organomet. Chem.* **1988**, *358*, C23.
(11) Ciani, G.; Sironi, A. *J. Organomet. Chem.* **1983**, *241*, 385.

10.1021/ic0007355 CCC: $20.00
Published on Web 07/04/2001

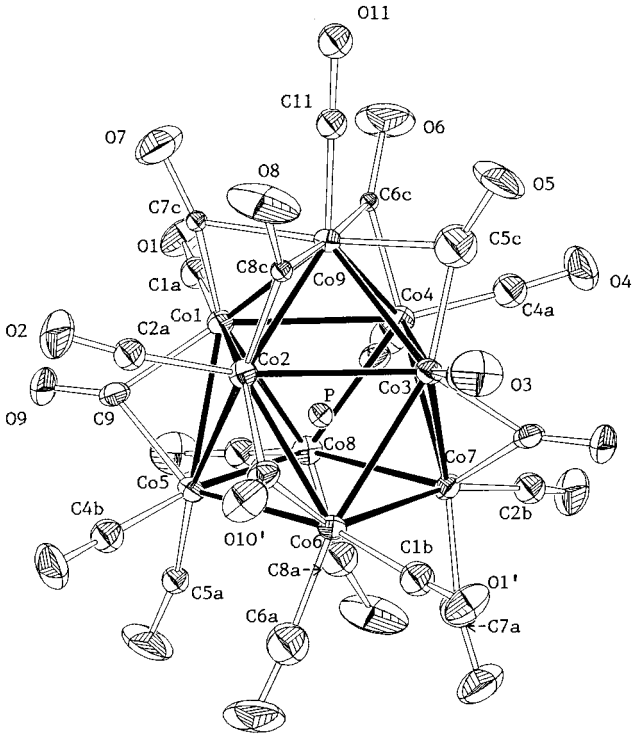

Figure 1. ORTEP drawing of the anion $[Co_9(\mu_8\text{-}P)(CO)_{21}]^{2-}$ (**1**). The carbonyl ligands are indicated by the labels of their oxygen atoms.

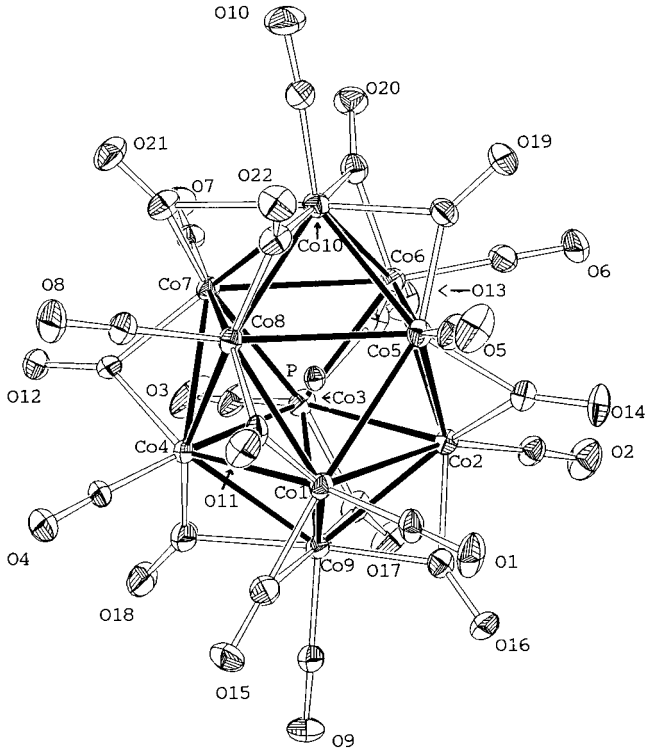

Figure 2. ORTEP drawing of the anion $[Co_{10}(\mu_8\text{-}P)(CO)_{22}]^{3-}$ (**2**). The carbonyl ligands are indicated by the labels of their oxygen atoms.

the paramagnetic silicide $[Co_9Si(CO)_{21}]^{2-}$ anion.[12] In addition, anion **2** is the first fully characterized example of a bicapped square antiprismatic carbonyl cluster of a first row transition metal.

Results

Synthesis and Reactivity. The $[Co_9P(CO)_{21}]^{2-}$ anion (**1**) was synthesized with a two step reaction; in the first step a tetrahydrofuran (THF) solution of $Na[Co(CO)_4]$ and PCl_5 in a 6:1 molar ratio is refluxed for a prolonged period of time to give a mixture of anions which, on the basis of the IR spectrum, have a charge/metal atom ratio higher than 2:9. In the second step, this mixture is exposed to a CO atmosphere, which causes disproportionation of all the species present to **1**, $[Co(CO)_4]^-$, and a trace of $[Co_6P(CO)_{16}]^-$. Separation of the $[Co_9P(CO)_{21}]^{2-}$ anion from this mixture is achieved by precipitation of the potassium salts from water, which leaves behind the $[Co(CO)_4]^-$ anion in the mother liquor. A metathesis of the potassium salt with PPh_4Br in methanol leaves the more soluble $[Co_6P(CO)_{16}]^-$ anion in solution. The anion **1** is also formed in the early stages of the pyrolysis of $K[Co_6P(CO)_{16}]$ or $(NMe_4)[Co_6P(CO)_{16}]$ in diglyme at 130 °C. Crystals suitable for X-ray analysis were obtained by layering a 0.4% solution of PPh_4Br in propan-2-ol over a methanolic solution of the potassium salt and leaving the solvents to diffuse. The dark-brown THF solution of the $[PPh_4]^+$ salt shows IR bands at 2001vs, 1980 sh, and 1808 m cm^{-1}.

The $[Co_{10}P(CO)_{22}]^{3-}$ anion (**2**) was obtained by the reaction of **1** with an excess of $[Co(CO)_4]^-$ in refluxing THF. The anhydrous sodium salt Na_3**2** is sparingly soluble in THF, and it precipitates off partially from the hot solution and almost completely on cooling at room temperature; other more reduced byproducts remain in solution. Crystals of the benzyltrimethylammonium ($[NMe_3Bz]^+$) salt suitable for X-ray analysis were obtained by layering a solution of $[NMe_3Bz]Cl$ in propan-2-ol over a methanol solution of the sodium salt. The $[NMe_3Bz]^+$ salt is insoluble in THF, but soluble in MeCN and acetone with a dark-brown color. The anhydrous sodium salt is sparingly soluble in THF, but becomes soluble on addition of trace amounts of water. The IR spectrum of the MeCN solution of the $[NMe_3Bz]_3$**2** salt shows bands at 1985 vs and 1778 m cm^{-1}. The anion reacts slowly with CO to give a mixture of $[Co_9P(CO)_{21}]^{2-}$ and $[Co(CO)_4]^-$.

Description of the Structures. The crystal structure of the compound $[PPh_4]_2$**1** consists of the packing of discrete $[Co_9P(CO)_{21}]^{2-}$ anions and cations in a 1:2 ratio. The anions lie on crystallographic inversion centers, so they must be disordered. The disorder doubles the number of cobalt atoms of the square antiprism, which is often observed within cluster species of similar geometry and can be easily rationalized, as described in the Experimental Section.

The structure of compound $[NMe_3Bz]_3$**2** contains two crystallographically independent $[Co_{10}P(CO)_{22}]^{3-}$ anions (labeled A and B) and six benzyltrimethylammonium cations in the asymmetric unit, separated by normal van der Waals contacts.

The structures of the anions $[Co_9P(CO)_{21}]^{2-}$ (**1**) and $[Co_{10}P(CO)_{22}]^{3-}$ (**2**) are illustrated in Figures 1 and 2, and relevant bond distances and angles are reported in Tables 1 and 2, respectively. A comparison of bond parameters within the known square antiprismatic cluster species containing interstitial heteroatoms is given in Table 3.

The anion $[Co_9P(CO)_{21}]^{2-}$, of overall idealized C_4 symmetry, contains a monocapped square antiprismatic Co_9 cluster with the phosphorus atom occupying the cavity of the cluster.

Of the CO ligands, 13 are terminally bonded and 8 bridge Co−Co edges. The metal atoms of the uncapped square face bear two terminal carbonyl ligands, the other Co atoms each have only one such ligand (overall mean Co−C and C−O for terminal CO groups: 1.79 and 1.16 Å). Four of the edge

(12) Mackay, V. M.; Nicholson, B. K.; Robinsin, W. T.; Sims, A. W. *J. Chem. Soc., Chem. Commun.* **1984**, 1276.

Table 1: Selected Bond Distances (Å) and Angles (Deg) for $[Co_9P(CO)_{21}]^{2-}$ (**1**)

Co1−Co2	2.831(4)	Co4−Co7	2.675(4)
Co2−Co3	2.829(5)	Co4−Co8	2.587(5)
Co1−Co4	2.811(5)	Co5−Co6	2.785(5)
Co3−Co4	2.848(4)	Co6−Co7	2.780(5)
Co1−Co5	2.585(4)	Co5−Co8	2.776(5)
Co1−Co8	2.653(4)	Co7−Co8	2.797(4)
Co2−Co5	2.677(4)	Co1−Co9	2.560(4)
Co2−Co6	2.601(4)	Co2−Co9	2.553(4)
Co3−Co6	2.661(4)	Co3−Co9	2.563(4)
Co3−Co7	2.587(4)	Co4−Co9	2.536(4)
Co1−P	2.252(3)	Co6−P	2.232(3)
Co2−P	2.211(3)	Co7−P	2.288(3)
Co3−P	2.246(3)	Co8−P	2.299(3)
Co4−P	2.280(3)	Co9···P	2.608(3)
Co5−P	2.247(3)		
Co1−C1A	1.80(1)	Co5−C4B	1.85(3)
Co6−C1B	1.90(3)	Co5−C5A	1.80(2)
Co2−C2A	1.80(2)	Co6−C6A	1.80(2)
Co7−C2B	1.76(3)	Co7−C7A	1.80(2)
Co3−C3A	1.80(2)	Co8−C8A	1.80(2)
Co8−C3B	1.68(3)	Co9−C11	1.70(2)
Co4−C4A	1.80(2)		
Co3−C5C	1.86(5)	Co1−C9	1.93(1)
Co9−C5C	2.01(5)	Co5−C9	1.96(1)
Co4−C6C	1.79(2)	Co3−C9′	1.89(1)
Co9−C6C	2.04(2)	Co7−C9′	1.97(1)
Co1−C7C	1.81(2)	Co4−C10	1.87(1)
Co9−C7C	2.10(2)	Co8−C10	1.91(1)
Co2−C8C	1.76(2)	Co2−C10′	1.94(1)
Co9−C8C	2.08(2)	Co6−C10′	1.98(1)

Table 2: Selected Bond Distances (Å) and Angles (deg.) for $[Co_{10}P(CO)_{22}]^{3-}$ (**2**) in the Two Independent Anions (A and B)

	A	B		A	B
Co1−Co2	2.814(2)	2.856(2)	Co1−C1	1.759(13)	1.745(10)
Co2−Co3	2.898(2)	2.819(2)	Co2−C2	1.763(12)	1.714(13)
Co3−Co4	2.797(2)	2.825(2)	Co3−C3	1.742(13)	1.760(9)
Co1−Co4	2.762(2)	2.862(2)	Co4−C4	1.730(11)	1.760(11)
Co5−Co6	2.833(2)	2.809(1)	Co5−C5	1.769(12)	1.751(7)
Co6−Co7	2.824(2)	2.765(2)	Co6−C6	1.734(12)	1.779(11)
Co7−Co8	2.775(2)	2.825(1)	Co7−C7	1.765(9)	1.745(8)
Co5−Co8	2.826(2)	2.830(2)	Co8−C8	1.728(13)	1.735(12)
Co1−Co5	2.700(2)	2.680(2)	Co9−C9	1.758(11)	1.743(11)
Co1−Co8	2.582(2)	2.563(2)	Co10−C10	1.726(12)	1.757(11)
Co2−Co5	2.556(2)	2.570(2)	Co1−C11	1.916(11)	1.878(12)
Co2−Co6	2.708(2)	2.709(2)	Co8−C11	1.874(10)	1.884(9)
Co3−Co6	2.546(2)	2.578(2)	Co4−C12	1.885(12)	1.911(10)
Co3−Co7	2.648(2)	2.664(2)	Co7−C12	1.921(9)	1.902(9)
Co4−Co7	2.587(2)	2.567(2)	Co3−C13	1.880(9)	1.938(9)
Co4−Co8	2.681(2)	2.684(2)	Co6−C13	1.910(10)	1.876(9)
Co1−Co9	2.664(2)	2.548(2)	Co2−C14	1.912(10)	1.905(9)
Co2−Co9	2.535(2)	2.596(2)	Co5−C14	1.908(13)	1.881(13)
Co3−Co9	2.562(2)	2.650(2)	Co1−C15	1.777(10)	1.887(10)
Co4−Co9	2.598(3)	2.568(2)	Co9−C15	2.514(10)	1.992(10)
Co5−Co10	2.567(2)	2.579(2)	Co2−C16	1.845(10)	1.859(10)
Co6−Co10	2.557(2)	2.589(2)	Co9−C16	1.981(12)	1.988(11)
Co7−Co10	2.626(2)	2.607(2)	Co3−C17	1.873(14)	1.775(13)
Co8−Co10	2.602(3)	2.581(2)	Co9−C17	1.956(9)	2.434(10)
Co1−P	2.264(2)	2.264(2)	Co4−C18	1.795(12)	1.834(13)
Co2−P	2.245(3)	2.260(3)	Co9−C18	2.111(14)	2.120(11)
Co3−P	2.258(2)	2.278(2)	Co5−C19	1.861(10)	1.845(10)
Co4−P	2.253(3)	2.264(3)	Co10−C19	1.968(13)	2.070(10)
Co5−P	2.263(3)	2.250(2)	Co6−C20	1.809(12)	1.843(11)
Co6−P	2.244(2)	2.276(2)	Co10−C20	2.063(8)	2.036(9)
Co7−P	2.282(3)	2.265(3)	Co7−C21	1.749(13)	1.832(12)
Co8−P	2.271(3)	2.259(3)	Co10−C21	2.378(13)	2.127(11)
Co9···P	2.708(3)	2.685(3)	Co8−C22	1.830(10)	1.835(10)
Co10···P	2.734(3)	2.747(3)	Co10−C22	2.004(9)	2.016(9)

bridging ligands span alternate interlayer edges connecting the squares and are almost symmetrical (mean Co−C and C−O: 1.93 and 1.16 Å); the other four CO groups bridge the edges of the cap and are markedly asymmetric, with quite longer contacts with Co9 (mean Co−C short, Co−C long, and C−O of 1.80, 2.06, and 1.27 Å, respectively).

Table 3: Relevant Mean Bond Distances (Å) within Uncapped, Monocapped, and Bicapped Square Antiprismatic Cluster Compounds

compound	M−M (intra)	M−M (inter)	M−M (cap)	M−M (all)	M−E[a]
$[Co_8C(CO)_{18}]^{2-}$[b]	2.505	2.544	−	2.524	1.99/2.15
$[Ni_8C(CO)_{16}]^{2-}$[c]	2.477	2.627	−	2.552	2.08
$[Co_9Si(CO)_{21}]^{2-}$[d]	2.874	2.640	2.613	2.728	2.299
$[Co_9P(CO)_{21}]^{2-}$[e]	2.807	2.628	2.553	2.685	2.256
$[Ni_9C(CO)_{17}]^{2-}$[c]	2.489	2.612	2.526	2.546	2.09
$[Co_{10}P(CO)_{22}]^{3-}$[e]	2.820	2.626	2.589	2.678	2.262
$[Ru_8P(CO)_{19}(Bz)]$[f]	2.914	2.891	−	2.902	2.39
$[Rh_9P(CO)_{21}]^{2-}$[g]	2.984	2.883	2.880	2.906	2.425
$[Rh_{10}P(CO)_{22}]^{3-}$[h]	3.007	2.864	2.851	2.907	2.435
$[Rh_{10}S(CO)_{22}]^{2-}$[i]	3.026	2.862	2.853	2.914	2.440
$[Rh_{10}As(CO)_{22}]^{3}$[j]	3.119	2.896	2.869	2.961	2.502

[a] Bonds involving the interstitial heteroatoms. [b] Reference 14. [c] Ceriotti, A., Longoni, G., Manassero, M., Perego M., and Sansoni, M., *Inorg. Chem.* **1985**, *24*, 117. [d] Reference 12. [e] This work. [f] Bz = μ-η^1,η^6-$CH_2C_6H_5$; Bullock, L. M., Field, J. S., Haines, R. J., Minshall, E., Moore, M. H., Mulla, F., Smit D. N., and Steer, L. M.; *J. Organomet. Chem.* **1990**, *381*, 429. [g] Reference 2. [h] Reference 3. [i] Ciani, G., Garlaschelli, L., Sironi A., and Martinengo, S. *J. Chem. Soc. Chem. Commun.* **1981**, 563. [j] Reference 4.

The Co−Co bond lengths display a pattern which is usual for these square antiprismatic clusters (see Table 3). There are five classes of metal−metal bonds: i) those within the uncapped square (4, mean 2.784 Å), ii) interlayer carbonyl bridged bonds (4, mean 2.590 Å), iii) interlayer carbonyl unbridged bonds (4, mean 2.666 Å), iv) those within the capped square (4, mean 2.830 Å), v) those involving the capping atom Co9 (4, mean 2.553 Å).

The metal cluster and the ligand geometry are similar to those present in the paramagnetic $[Co_9Si(CO)_{21}]^{2-}$ anion.[12] In this species, the five above Co−Co bond lengths, grouped according to the five aforementioned classes, show the following average values: i) 2.808(1), ii) 2.593(1), iii) 2.688(1), iv) 2.940(1), and v) 2.613(1) Å. The class iv mean bond length exhibits the major difference between the phosphide and the silicide species. Another minor difference consists of the fact that the interlayer bridging CO ligands are slightly more asymmetric in the silicide [Δ(M−C) 0.11 Å] than in the phosphide [Δ(M−C) 0.04 Å].

A quite different ligand geometry, on the other hand, was found in $[Rh_9P(CO)_{21}]^{2-}$:[2] the four terminal CO groups, that are axially bonded to the uncapped square face metals in the two Co_9 species, in the Rh_9 anion become asymmetric double bridges on the four edges of the same square face. Moreover in the rhodium species, the four CO groups bridging the interlayer edges are markedly asymmetric [with longer contacts with the uncapped face metals, Δ(M−C) ca. 0.27 Å], and the interlayer bridged and unbridged edges show very similar bond lengths (mean Rh−Rh 2.874 and 2.892 Å, respectively).

The Co−P interactions involving the metals of the uncapped square face are slightly longer (mean 2.266 Å) than those involving the metals of the capped face (mean 2.247 Å); the same feature implying the heteroatom was also observed in the related Co_9Si and Rh_9P species. The P atom is 0.10 Å closer to the plane of the capped square. The Co9−P distance, 2.608(3) Å, represents a weak interaction, being ca. 15% longer than the other 8 contacts (overall mean 2.256 Å), and is comparable with the corresponding Co−Si interaction in $[Co_9Si(CO)_{21}]^{2-}$, 2.527(4) Å. On the other hand, the Rh−P distance involving the capping rhodium atom in $[Rh_9P(CO)_{21}]^{2-}$, 3.057(3) Å, is definitely nonbonding, being ca. 26% longer than the other

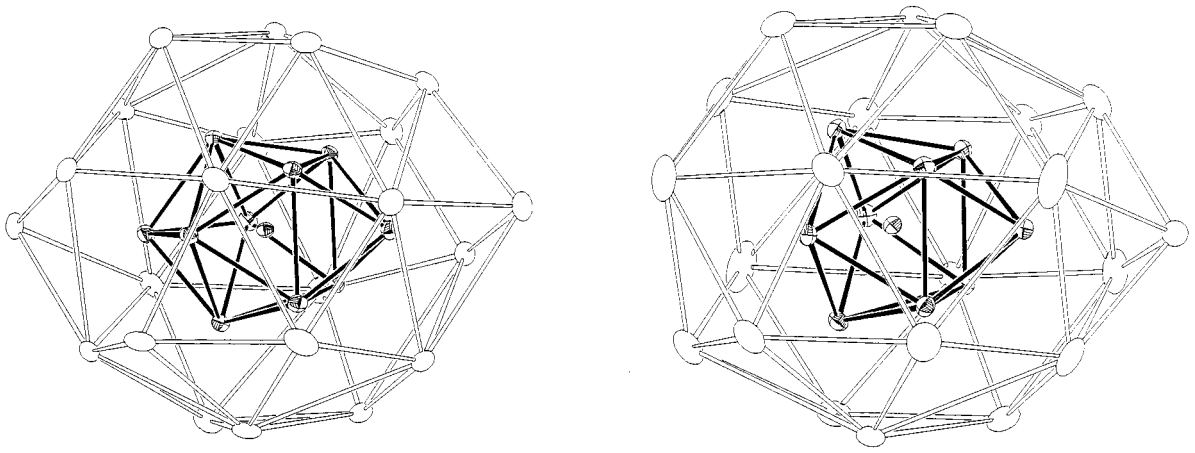

Figure 3. Oxygen atoms polyhedra for anions **1** and **2**.

Rh−P contacts (mean 2.425 Å). An analysis of the bond parameters in the Co_9Si and Co_9P species (see Table 3) shows slightly longer overall mean M−M and M−E bond lengths in the silicide, in agreement with the expected greater radius of Si versus P.

The anion $[Co_{10}P(CO)_{22}]^{3-}$, of overall idealized D_4 symmetry, contains a closo bicapped square antiprismatic cluster centered by the phosphide ligand. As mentioned above, this is the first example of such a cluster geometry structurally characterized for first row transition metals. The two independent anions (labeled A and B) exhibit very similar bond parameters. The structure of the $[Co_{10}P(CO)_{22}]^{3-}$ anion can be formally derived from that of the related $[Co_9P(CO)_{21}]^{2-}$ anion by inserting a $[Co(CO)]^-$ unit into its unique square face and allowing the bending of four nearby terminal carbonyl ligands (one for each metal atom of the square face) toward the incoming unit. Ideally, the overall carbonyl ligand disposition within the anion can be described as follows: there are 10 terminal CO ligands, one per metal atom (overall mean Co−C and C−O, 1.748 and 1.143 Å), and 12 edge bridging groups, 4 of which, as in anion **1**, are on alternate interlayer edges (symmetrical, overall mean Co−C and C−O, 1.899 and 1.174 Å) and 8 involved in asymmetric interactions with the two capping metals (with longer contacts with the caps; Co−C short and long contacts in the ranges 1.75−1.89 and 1.97−2.51 Å, respectively). Three of these CO groups, however, (one per cap, except for Co10B) seem to be mainly terminal ligands of the cobalt atoms of the squares, exhibiting only very weak interactions with the caps.

The Co−Co bond lengths belong to four classes: i) those within the square layers (8 in each independent anion, overall mean 2.820 Å), ii) interlayer carbonyl bridged bonds (4, overall mean 2.569 Å), iii) interlayer carbonyl unbridged bonds (4, overall mean 2.684 Å), iv) those within the caps (8, overall mean 2.589 Å). This trend is on line with the values found in the bicapped square antiprismatic rhodium species reported in Table 3.

The P atoms occupy the centers of the square antiprismatic holes and exhibit very similar contacts with the eight metals defining such cavities (overall mean Co−P, 2.262 Å); the Co−P interactions with the capping metal atoms are much longer (mean 2.718 Å) and definitely nonbonding.

In the study of cluster compounds with interstitial heteroatoms, the criterion of the radius ratio r_E/r_M is often useful for the prediction of the more suitable cluster geometry. The structure of the $[Co_6P(CO)_{16}]^-$ anion[11] was indicative of the fact that a phosphorus atom cannot be located inside an octahedral or trigonal prismatic cage of cobalt atoms, while such an interstitial species can be contained inside a trigonal prism (somewhat elongated in the 3-fold axis direction) of osmium atoms, as in $[Os_6P(CO)_{18}]^-$ or $[Os_6P(CO)_{18}(AuPPh_3)]$.[13] A theoretical radius ratio r_E/r_M of 0.646 is associated with a regular square antiprismatic cavity. However, the structures of the compounds reported in Table 3 show that the square antiprismatic clusters (and their capped derivatives) possess a certain elasticity which enables them to accommodate, via some distortions, different kinds of interstitial atoms showing different r_E/r_M values. The structural data indicate that usually the average M−E contacts are shorter than the sum of the relevant covalent radii and, to achieve a better stabilization for the central heteroatom, the clusters can exhibit: i) drastic distortions of the metallic skeleton, implying a decrease in the number of cluster valence electrons with respect to the value associated with the square antiprismatic geometry, as in $[Co_8C(CO)_{18}]^{2-}$;[14] ii) elongation of the carbonyl unbridged M−M edges, either in axial direction, as in the Ni_8 and Ni_9 species, or in equatorial direction, as in the cobalt and rhodium M_9 and M_{10} species; iii) variable extents of interaction of the capping metals with the central heteroatom. However, there are limits that cannot be exceeded. In the case of rhodium, on passing from As to Sb, an icosahedral rather than a square antiprismatic cage results are more suitable (as in $[Rh_{12}Sb(CO)_{27}]^{3-}$). It also could be suggested that for cobalt, on passing from Si or P to Ge or As, a cavity larger than that of a square antiprism should be more adequate; indeed an icosahedral metallic frame was found in the case of $[Ni_{10}Ge(CO)_{20}]^{2-}$ and $[Ni_{12}Ge(CO)_{22}]^{2-}$.[15]

Finally, all the Co and Rh monocapped and dicapped square antiprismatic species reported in Table 3 exhibit similar carbonyl dispositions. The polyhedron formed by the oxygen atoms in the M_{10} species (see Figure 3b) shows an idealized D_{4h} symmetry, higher than that of the whole anions (D_4 idealized symmetry), and for the M_9 species, the oxygen polyhedron is very similar but lacks of one of the two axial vertexes (Figure 3a). Inversion of the whole M_{10} anions about their central point (coincident with location of the interstitial heteroatom) leaves the oxygen polyhedron and, therefore, the intermolecular contacts essentially unchanged but gives rise to disorder for the anion (involving the metal atoms and most of the carbon atoms,

(13) Colbran, S. B.; Hay, C. M.; Johnson, B. F. G.; Lahoz, F. J.; Lewis, J.; Raithby, P. R. *J. Chem. Soc., Chem. Commun.* **1986**, 1766.
(14) Albano, V. G.; Chini, P.; Ciani, G.; Martinengo, S.; Sansoni, M. *J. Chem. Soc., Dalton Trans.* **1978**, 463.
(15) Ceriotti, A.; Demartin, F.; Heaton, B. T.; Ingallina, P.; Longoni, G.; Manassero, M.; Marchionna, M.; Masciocchi, N. *J. Chem. Soc., Chem. Commun.*, **1989**, 786.

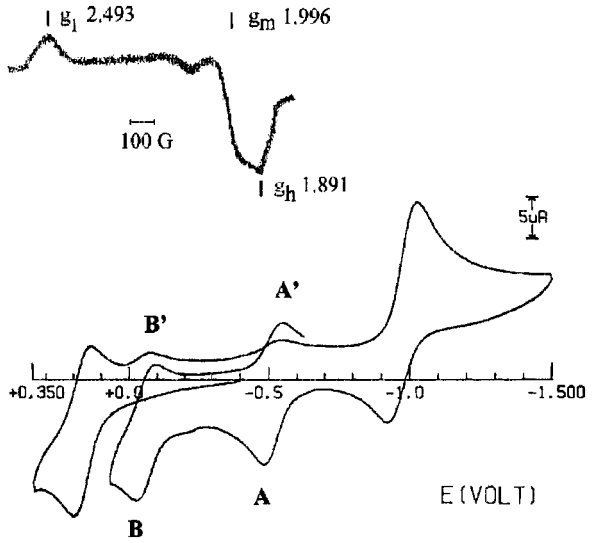

Figure 4. Bottom: cyclic voltammogram recorded at a platinum electrode on a MeCN solution containing $[Co_9P(CO)_{21}]^{2-}$ (6×10^{-4} mol dm^{-3}) and $[NEt_4][ClO_4]$ (0.1 mol dm^{-3}). Scan rate 0.2 Vs^{-1}. Inset: X-Band EPR spectrum recorded at 105 K after anodic one-electron oxidation at 153 K.

see Experimental). A similar situation occurs for the M_9 anions. Disorder, in fact, is observed in three out of the seven crystal structures of anions of this type in Table 3: $[Co_9P(CO)_{21}]^{2-}$, $[Rh_{10}P(CO)_{22}]^{3-}$, and $[Rh_{10}S(CO)_{22}]^{2-}$. It is not simple to envisage the factors which can favor order instead of disorder, and the nature of the counterions seems to not give clear indications.

Electrochemistry and Coupled EPR Spectroscopy. The cyclic voltammetric response illustrated in Figure 4 shows that the 130-CVE dianion $[Co_9P(CO)_{21}]^{2-}$ in acetonitrile solution undergoes either an anodic process ($E^{\circ\prime} = +0.16$ V), or a cathodic process ($E^{\circ\prime} = -1.00$ V), both of which are partially chemically reversible. In addition, both of the redox processes give rise to the two new peak systems A/A′ and B/B′, which are localized at intermediate potential values ($E^{\circ\prime} = -0.06$ V, -0.51 V, respectively). This means that the chemical complications accompanying either the oxidation or the reduction processes generate the same redox congeners.

The determination of the number of electrons involved in each of the primary redox changes was attempted by controlled potential coulometry, but the electrolysis current did not decay significantly. Presumably, internal electron transfer occurring in the long times of macroelectrolysis tended to regenerate the original species. For instance, a hydrodynamic voltammetric test,[16] at an electrode with periodical renewal of the diffusion layer, performed after the consumption of about five electrons/molecule in the anodic step indicated that less than 20% of the original species underwent oxidation. An indication that the anodic step involves one-electron removal was obtained by EPR spectroscopy on the product obtained by controlled potential coulometry ($E_w = +0.4$ V) at low temperature (-20 °C). As the inset in Figure 4 shows, the X-band EPR spectrum, recorded at liquid nitrogen temperature (T = 105 K) on the solution resulting from about one-electron oxidation, exhibits broad and partially resolved rhombic (aniso) features ($g_l > g_m > g_h \neq g_{electron} = 2.0023$), slightly overlapped in the high field region, which can be usefully interpreted in terms of the $S = {}^1/_2$ Electron Spin Hamiltonian $H = g\beta HS + AIS$. The anisotropic line shape

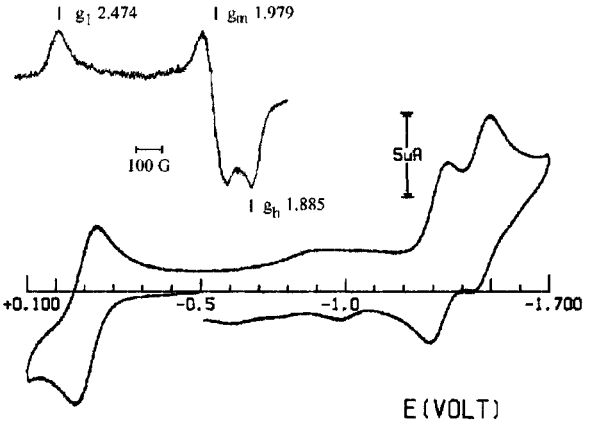

Figure 5. Bottom: cyclic voltammogram recorded at a platinum electrode on a MeCN solution containing $[Co_{10}P(CO)_{22}]^{3-}$ (5×10^{-4} mol dm^{-3}) and $[NEt_4][ClO_4]$ (0.1 mol dm^{-3}). Scan rate 0.2 Vs^{-1}. Inset: X-Band EPR spectrum recorded at 105 K after anodic one-electron oxidation at 153 K.

analysis makes evident the metallic character of the likely electrogenerated paramagnetic monoanion $[Co_9P(CO)_{21}]^{-}$, thus suggesting that the unpaired electron is mainly delocalized on the Co_9 cage. No direct evidence for hyperfine (hpf) interactions of the unpaired electron, either with the magnetically active cobalt nuclei (I−Co = 7/2) or with the phosphorus nucleus (I−P = $^1/_2$), was obtained; this is likely due to the actual line width, ΔH_{aniso}, largely overlapping the eventual hpf Co/P interactions. The relevant paramagnetic parameters calculated by best fit computer treatment[17] are:

$$g_l = 2.493 \pm 0.005;\ g_m = 1.996 \pm 0.005;\ g_h = 1.891 \pm 0.005;\ \Delta g = g_l - g_h = 0.602 \pm 0.005$$

$$\langle g \rangle = (g_l + g_m + g_h)/3 = 2.117 \pm 0.005$$

Upon increasing the temperature, the spectral intensity decreases, and at the glassy-fluid transition the anisotropic EPR signal is lost. In confirmation of the instability of the monoanion, freezing this fluid solution does not restore the original EPR signal.

Since the generation of the transient paramagnetic species confirms the one-electron nature of the anodic step at $E^{\circ\prime} = +0.16$ V, on the basis of the relative current intensities, we assign the cathodic step occurring at $E^{\circ\prime} = -1.00$ V as a single two-electron process.

The secondary species responsible for the appearance of the reversible peak-systems A/A′ and B/B′ was tentatively attributed to degradation to the phosphide cluster monoanion $[Co_6P(CO)_{16}]^{-}$. Indeed, such monoanion undergoes a quite different redox pathway, consisting of a partially reversible one-electron reduction (coulometrically measured) at $E^{\circ\prime} = +0.70$ V and an irreversible one-electron oxidation at $E_p = +0.16$ V. Further chemical investigations are needed to identify the new electrogenerable species. According to these findings, it is unlikely that paramagnetic $[Co_9P(CO)_{21}]^{-}$ will be isolated, although the isoelectronic silicide $[Co_9Si(CO)_{21}]^{2-}$ is stable. It is therefore evident that interstitial silicon, but not phosphorus, confers redox flexibility to the cluster cage.

The cyclic voltammogram for the 142-CVE trianion, $[Co_{10}P(CO)_{22}]^{3-}$, is shown in Figure 5. It exhibits a redox pattern similar to that of $[Co_9P(CO)_{21}]^{2-}$, in that it undergoes either a one-electron oxidation ($E^{\circ\prime} = -0.10$ V) or a two-electron

(16) Lo Schiavo, S.; Bruno, G.; Zanello, P.; Laschi, F.; Piraino, P. *Inorg. Chem.*, **1997**, *36*, 1004.

(17) Lozos, G. P.; Hoffmann, G. B.; Franz, C. G. *Q. C. P. E.* **1973**, *263*, 11.

reduction, but, in variance with the latter, the two-electron reduction proceeds through two slightly separated one-electron steps ($E^{\circ\prime} = -1.32$ V, -1.47 V, respectively). Cyclic voltammograms recorded at scan rates increasing from 0.02 to 1.00 Vs^{-1} show that the chemical reversibility of the redox changes is limited.[18] The chemical reactions following the electron transfers do not generate the previous secondary species which was responsible for the peaks at A/A′ and B/B′. A further multielectron process, irreversible in character and not shown in the figure, is present at $E_p = +0.37$ V. The number of electrons involved in the most relevant processes has been deduced from EPR spectroscopy, because controlled potential coulometry failed. The inset in Figure 5 shows the EPR spectrum recorded at liquid nitrogen temperature after the consumption of about one electron/molecule in the anodic step ($E_w = +0.1$ V) at low temperature (-20 °C). The EPR line shape analysis was suitably carried out in terms of the $S = {}^1/_2$ Electron Spin Hamiltonian. The relevant paramagnetic parameters are:

$$g_l = 2.474 \pm 0.005;\ g_m = 1.979 \pm 0.005;\ g_h = 1.885 \pm 0.005;\ \Delta g = g_l - g_h = 0.586 \pm 0.005$$

$$\langle g \rangle = (g_l + g_m + g_h)/3 = 2.113 \pm 0.005$$

The line shape displays a well resolved rhombic structure, and the parameters are consistent with the metal nature of the unpaired electron in the dianion $[Co_{10}P(CO)_{22}]^{2-}$, as confirmed by the large overall ΔH_{aniso} value. As with $[Co_9P(CO)_{21}]^-$, an increased temperature attenuates the EPR signal which disappears at the glassy-fluid transition, but, refreezing the fluid solution quantitatively restores the anisotropic signal, indicating significant stability for the electrogenerated dianion.

Experimental Section

All operations were carried out under a nitrogen atmosphere using Schlenk-tube techniques. Tetrahydrofuran was purified by distillation from Na−benzophenone ketyl, and all other solvents were distilled and stored under nitrogen. IR spectra were recorded on a Perkin-Elmer 781 spectrophotometer using 0.1 mm CaF_2 cells purged with nitrogen.

Materials and apparatus for electrochemistry and coupled EPR spectroscopy have been described elsewhere.[16] All of the potential values are referred to the Saturated Calomel Electrode (SCE). Under the present experimental conditions, the one electron oxidation of ferrocene occurs at +0.38 V versus SCE.

The external magnetic field H_0 for EPR spectroscopy was calibrated by using a DPPH powder sample ($g_{DPPH} = 2.0036$).

Synthesis of $[Co_9P(CO)_{21}]^{2-}$. A stirred solution of $Na[Co(CO)_4]$ (1.197 g) in 35 mL of THF was treated under nitrogen at −70 °C with a solution of 0.212 g of PCl_5 in 15 mL of THF. After the addition, the cooling bath was removed, and the solution was allowed to warm at room temperature; the color changed to orange-brown, while evolution of CO was observed. The reaction vessel was equipped with a coldfinger, and the solution was heated at reflux in an oil bath thermostated at 100 °C. Every hour the tube was briefly opened in nitrogen flow in order to remove the evolved CO and to take an IR spectrum of the solution. Reflux was continued until the terminal COs stretching bands were in the range 1995−1975 cm^{-1} and the band of $[Co(CO)_4]^-$ had almost disappeared (about 6 h). The resulting solution was filtered from some black material and then exposed overnight to a CO atmosphere. This caused decomposition of all the products present in solution to a mixture of $[Co_9P(CO)_{21}]^{2-}$, $[Co(CO)_4]^-$, and some $[Co_6P(CO)_{16}]^-$, as indicated by the IR spectrum. The solution was concentrated in a vacuum to about 6 mL and then treated with 40 mL of *n*-heptane and concentrated to 15 mL to give a black precipitate and a pale orange solution. After removal of the orange mother liquor (containing a trace of a neutral species presently under investigation and showing IR bands at 2037 vs, 2028 s, 2007 s, and 1880 m cm^{-1}), the residue was washed with *n*-heptane and vacuum dried. The solid was dissolved in 50 mL of water, the resulting solution was treated with 25 g of KBr and then left to crystallize overnight. The precipitate was filtered, washed with a saturated aqueous solution of KBr, and vacuum dried. The potassium salt isolated can be used for the synthesis of $[Co_{10}P(CO)_{22}]^{3-}$ or converted to the corresponding bulky cations salts.

The $[PPh_4]^+$ salt was obtained by extraction of the potassium salt with 20 mL of methanol, filtration, and dropwise addition, while stirring, of a solution of $[PPh_4]Br$ in 10 mL of MeOH. The crystalline precipitate was filtered, washed twice with 5 mL of propan-2-ol, then washed with water, then again with propan-2-ol, and finally vacuum dried to give about 0.6 g of product (yield 32%, calculated on P). The mother liquor contains traces of $[Co_6P(CO)_{16}]^-$. Calc. for $C_{69}H_{40}Co_9O_{21}P_3$: C, 45.3; H, 2.2%. Found: C, 45.0; H, 1.8%.

Synthesis of $[Co_{10}P(CO)_{22}]^{3-}$. A stirred solution of the crude $K_2[Co_9P(CO)_{21}]$ (0.26 g, 0.211 mmol) and a 5-fold excess of $Na[Co(CO)_4]$ (0.2 g) in THF (26 mL) was heated at reflux in an oil bath kept at 100 °C, taking an IR spectrum every hour. Reflux was continued until the terminal CO's bands of the starting anion were replaced by bands at about 1988 cm^{-1}. Some of the product separated out during the reaction as a black precipitate (separation is more abundant on cooling at room temperature and occurs also into the IR cell while taking the spectra). At the end, the reaction mixture was left to crystallize for 2 days at room temperature. The separated needles were filtered, washed with some THF, and vacuum dried. The product was transformed into the corresponding benzyltrimethylammonium salt by dissolution in MeOH and layering with a 0.4% solution of $[NMe_3Bz]Cl$ in propan-2-ol. When the diffusion of the solvents was complete, the product was filtered, washed with propan-2-ol, water, again with 2-propanol, and vacuum dried. Yield: 0.2−0.3 g (about 75%). Calc. for $C_{52}H_{48}Co_{10}N_3O_{22}P$: C, 37.8; H, 2.87; N, 2.49%. Found: C, 38.1; H, 2.9; N, 2.4.

X-ray Structure Analysis. Dark prismatic specimens of $[PPh_4]_2$**1** and $[NMe_3CH_2Ph]_3$**2** were mounted on the tip of a thin glass fiber for X-ray examination and data collection. All data were collected, at room temperature, on a CAD4 diffractometer with graphite monochromated Mo Kα radiation ($\lambda = 0.71073$ Å). Unit cell parameters were obtained by least-squares refinement of the angular settings of 25 intense reflections having $8 < \theta < 12°$. Crystal data and intensity collection parameters are reported in Table 4. Intensity data were collected in the ω scan mode with $3 < \theta < 24$ and $3 < \theta < 23°$, respectively. Three standard reflections were monitored every hour and showed a gradual decrease of the scattering power of the crystals, which was evaluated as about 6% and 10% for $[PPh_4]_2$**1** and $[NMe_3CH_2Ph]_3$**2**, respectively, at the end of the data collection. The full data sets were corrected for Lorentz, polarization, decay, and absorption effects. An empirical

Table 4. Summary of Crystal Data

compound	$[PPh_4]_2$**1**	$[NMe_3CH_2Ph]_3$**2**
formula	$C_{69}H_{40}Co_9O_{21}P_3$	$C_{52}H_{48}Co_{10}N_3O_{22}P$
formula weight, amu	1828.4	1687.3
space group	$P2_1/n$ (No.14)	P-1 (No. 2)
a, Å	12.528(3)	11.452(3)
b, Å	14.711(5)	23.510(6)
c, Å	19.312(6)	25.606(4)
α, °		112.46(1)
β, °	93.68(2)	95.79(1)
γ, °		73.54(2)
V, Å^3	3552(3)	6110(4)
Z, D_{calc}, g cm^{-3}	2, 1.709	4, 1.834
radiation, Å	Mo Kα $\lambda = 0.71073$	Mo Kα $\lambda = 0.71073$
μ, cm^{-1}	21.8	27.4
θ range, deg	3−24	3−23
R[a]	0.065	0.041
Rw[b]	0.070	0.044

[a] $R = \sum(|F_o - k|F_c||)/\sum F_o$ [b] $Rw = [\sum w(F_o - k|F_c|)^2/\sum wF_o^2]$ - $w = 4F_o^2/\sigma^2(F_o^2)$; $\sigma(F_o^2) = [\sigma^2(I) + (pI)^2]^{(1/2)}$ − /LP

(18) Brown, E. R.; Sandifer, J. R. In *Physical Methods of Chemistry. Electrochemical Methods*; Rossiter, B. W.; Hamilton, J. F., Eds.; Vol. 2; Wiley: New York, 1986, Ch 4.

absorption correction was applied according to the method developed by North et al.[19] based on Ψ scans (Ψ 0−360°, every 10°) of three reflections having χ values near 90°. All crystallographic computations were carried out by using the SHELX program[20] and a IBM 3090 mainframe computer.

Solution and Refinement of the Structures. The initial location of the metal atoms were determined by three-dimensional Patterson function $[PPh_4]_2$**1** and Direct Methods (MULTAN)[21] $[NMe_3CH_2Ph]_3$**2**); the remaining lighter (P, C, N, and O) atoms were found by subsequent Fourier difference syntheses. Full matrix least-squares refinements (for $[PPh_4]_2$**1** vide infra) minimizing the function $\Sigma w(F_o - k|F_c|)^2$ were carried out until the largest shift in any parameter was less than 0.5σ. The contribution of the hydrogen atoms to the scattering factors was omitted. Individual weights were assigned according to the formula: $w = A/(\sigma^2(F) + BF^2)$, with $A = 2.2391/1.3089$ and $B = 0.001599/0.000879$ (Compounds $[PPh_4]_2$**1**/$[NMe_3CH_2Ph]_3$**2**). Scattering factors and anomalous dispersion terms were taken from ref 22. Final R, Rw, and esd values are reported in Table 4. Final atomic positional parameters are given in the Supporting Information for $[PPh_4]_2$**1** and $[NMe_3CH_2Ph]_3$**2**, respectively.

The $[Co_9P(CO)_{21}]^{2-}$ anion was found to be disordered about an inversion center, the overall crystal packing being dictated by the shape of the oxygen atoms envelope, which is very similar in the two "up" and "down" orientations of the metal core. Consequently, all metal atoms were given occupancy number of 0.5. Furthermore, assuming near coincidence of all oxygen atoms but one (the terminal carbonyl on the capping Co9 atom, with occupancy number of 0.5, all others being refined with unitary occupancies), the following disordered model has been chosen:

i) the edge bridging C9/C10/O9/O10 carbonyls, which are coincident in the two "up" and "down" orientations, although connected to two different couples of metal atoms, were given occupancy numbers of 1.0.

ii) the "axially bonded" CO ligands simultaneously behave as terminal and asymmetrically bridging COs on the uncapped/capped square faces of the central antiprism, respectively. A split carbon model (occupancy numbers of 0.5) for all these atoms was adopted. (A-labeled carbon atoms belong to terminal ligands, C-labeled ones to the bridging COs).

iii) the 'radially bonded' CO ligands behave as terminally bonded ligands for both metal core orientations. A split carbon model is again used. (A- and B-labeled carbon atoms belong to different sets of the terminal ligands)

iv) a constrained refinement for the terminal carbonyls with *A* label was performed, using the DFIX instruction of the SHELX package. The chosen values were: Co−C, 1.80; C−O, 1.15; Co···O, 2.95 Å; $s = 0.005$ Å.

Acknowledgment. We gratefully acknowledge the financial support of Cofinanziamento MURST 2000.

Supporting Information Available: Positional and thermal parameters for the structure determinations of complexes **1** and **2** (7 pages). (X-ray crystallographic files are not available in CIF format.) This material is available free of charge via the Internet at http://pubs.acs.org.

IC0007355

(19) North, A. C.; Phillips, D. C.; Scott Mathews, F. *Acta Crystallogr.* **1968**, *A24*, 351−359.
(20) Sheldrick, G. M. *SHELX76*, Program for crystal structure determination. University of Cambridge, England, 1976.
(21) Germain, G.; Main, P.; Woolfson, M. M. *Acta Crystallogr.* **1971**, *A27*, 368−372.
(22) Cromer, D. T. *International Tables for X-ray Crystallography*, Vol *4*. Birmingham: The Kynoch Press (present distributor Kluwer Academic Publishers: Dordrecht), **1974**, Table 2.3.1.